

# End-to-end Animal Image Matting

Jizhizi Li, Jing Zhang, Stephen J. Maybank, *Fellow, IEEE*, Dacheng Tao, *Fellow, IEEE*

**Abstract**—Extracting accurate foreground animals from natural animal images benefits many downstream applications such as film production and augmented reality. However, the various appearance and furry characteristics of animals challenge existing matting methods, which usually require extra user inputs such as trimap or scribbles. To resolve these problems, we study the distinct roles of semantics and details for image matting and decompose the task into two parallel sub-tasks: high-level semantic segmentation and low-level details matting. Specifically, we propose a novel Glance and Focus Matting network (GFM), which employs a shared encoder and two separate decoders to learn both tasks in a collaborative manner for end-to-end animal image matting. Besides, we establish a novel Animal Matting dataset (AM-2k) containing 2,000 high-resolution natural animal images from 20 categories along with manually labeled alpha mattes. Furthermore, we investigate the domain gap issue between composite images and natural images systematically by conducting comprehensive analyses of various discrepancies between foreground and background images. We find that a carefully designed composition route RSSN that aims to reduce the discrepancies can lead to a better model with remarkable generalization ability. Comprehensive empirical studies on AM-2k demonstrate that GFM outperforms state-of-the-art methods and effectively reduces the generalization error.

**Index Terms**—Image Matting, Deep Learning, Alpha Matte, Image Composition, Domain Gap

## 1 INTRODUCTION

IMAGE matting refers to extracting the foreground alpha matte from an input image, requiring both hard labels for the explicit foreground or background and soft labels for the transition areas. Specifically, animal matting that aims at extracting the foreground animal from an image, plays an important role in many applications, e.g., virtual reality, augmented reality, entertainment, etc. Different categories of animals have the diverse appearance and furry details, which lay a great burden on image matting methods. How to recognize the semantic foreground or background as well as extract the fine detail for end-to-end animal matting remains challenging. However, this research topic is under-explored in the image matting community.

For image matting, an image  $\mathbf{I}$  is assumed to be a linear combination of foreground  $\mathbf{F}$  and background  $\mathbf{B}$  via a soft alpha matte  $\alpha \in [0, 1]$ , i.e.,

$$\mathbf{I}_i = \alpha_i \mathbf{F}_i + (1 - \alpha_i) \mathbf{B}_i \quad (1)$$

where  $i$  denotes the pixel index. It is a typical ill-posed problem to estimate  $\mathbf{F}$ ,  $\mathbf{B}$ , and  $\alpha$  given  $\mathbf{I}$  from Eq. (1) due to the under-determined nature. To address this issue, previous matting methods adopt extra user input such as trimap [1] and scribbles [2] as priors to decrease the degree of unknown. Based on sampling neighboring known pixels [3], [4], [5] or defining an affinity matrix [6], the known alpha values (i.e., foreground or background) are propagated to the unknown pixels. Usually, some edge-aware smoothness constraints are used to make the problem tractable [2]. However, either the sampling or calculating affinity matrix is based on low-level color or structural features, which is not so discriminative at indistinct transition areas or fine edges. Consequently, their performance is sensitive to the size of

unknown areas and may suffer from fuzzy boundaries and color blending. To address this issue, deep convolutional neural network (CNN)-based matting methods have been proposed to leverage its strong representative ability and the learned discriminative features [1], [7], [8], [9], [10]. Although CNN-based methods can achieve good matting results, the prerequisite trimap or scribbles make them unlikely to be used in automatic applications such as the augmented reality of live streaming and film production. For animal images, the issue becomes even worse since it may take great effort to indicate the transition areas regarding their furry nature and occlusions by the living environment, e.g., grassland and trees, in consideration of their protective coloration.

To address this issue, end-to-end matting methods have been proposed [7], [8], [9], [10], [11] in recent years. Most of them can be categorized into two types. The first type shown in (i) of Figure 1(a) is a straightforward solution which is to perform global segmentation [12] and local matting sequentially, where the former aims at trimap generation [7], [11] or foreground/background generation [8] and the latter is image matting based on the trimap or other priors generated from the previous stage. The shortage of such a pipeline attributes to its sequential nature, since they may generate an erroneous semantic error which could not be corrected by the subsequent matting step. Besides, the separate training scheme in two stages may lead to a sub-optimal solution due to the mismatch between them. The second type is shown in (ii) of Figure 1(a), global information is provided as guidance while performing local matting. For example, coarse alpha matte is generated and used in the following matting network in [10] and in [9], spatial- and channel-wise attention is adopted to provide global appearance filtration to the matting network. Such methods avoid the problem of state-wise modeling and training but bring in new problems. Although global guidance is provided in an implicit way, it is challenging to generating alpha matte for both

J. Li, J. Zhang, and D. Tao are with the UBTECH Sydney Artificial Intelligence Centre, School of Computer Science, Faculty of Engineering, The University of Sydney, Sydney, Australia. S.J. Maybank is with the School of Computer Science and Information Systems, Birkbeck College, London, U.K. Corresponding author: Dacheng Tao (dacheng.tao@sydney.edu.au)

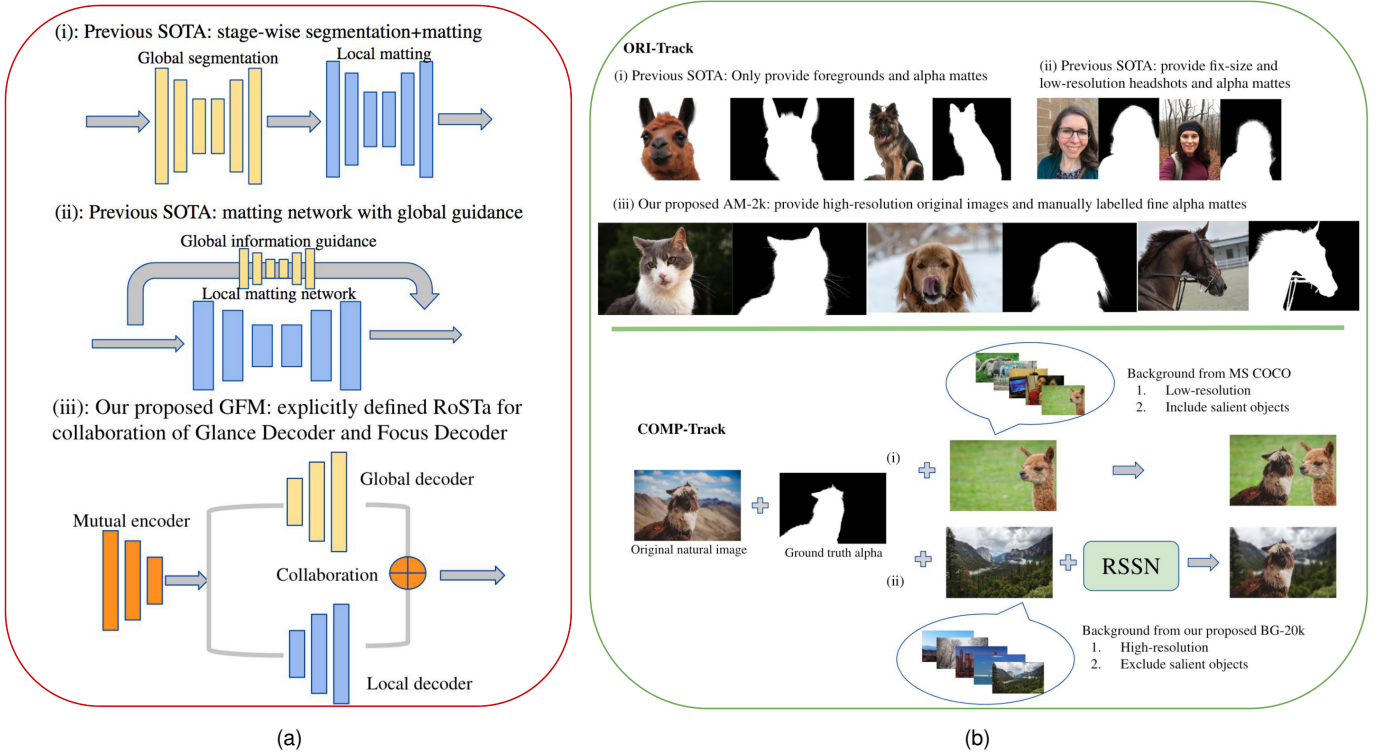


Fig. 1. (a) The comparison between SOTA end-to-end-matting methods in (i) and (ii) and our GFM in (iii). (b) The comparison between existing matting datasets and our proposed AM-2k as well as the comparison between existing composition methods and our RSSN.

foreground/background areas and transition areas simultaneously in a single network due to their distinct appearance and semantics. For animal matting, it is more difficult to generate reliable trimap and estimate accurate alpha matte that will challenge the above two pipelines due to the following two reasons. First, there are different categories of animals with diverse shapes, sizes, colors, and appearances in the animal matting task other than a single category in other matting tasks such as human portrait matting [7], [10], [11]. Second, the protective coloration of animals makes it hard to recognize the foreground and distinguish the animal fur from the background context. Thereby, how to design a novel framework to learn discriminative features and distinguish the semantic foreground/background from the fine details in the transition area for animal image matting remains challenging and under-explored.

Another challenge is the limitation of the current available matting dataset. As shown in Figure 1(b) ORI-Track, due to the laborious and costly labeling process, existing public matting datasets only have tens or hundreds of high-quality annotations [1], [8], [9], [11], [13]. They either only provide foregrounds and alpha mattes [1], [9] as in (i) of Figure 1(b) ORI-Track, or provide fix-size and low-resolution ( $800 \times 600$ ) headshots with inaccurate alpha mattes [11] generated by ensemble of existing matting algorithms as in (ii) of Figure 1(b) ORI-Track. Moreover, the number of animal samples in these datasets is even less (about 100 images). Due to the unavailability of original natural images, as shown in (i) of Figure 1(b) COMP-Track, a common practice for data augmentation in matting is to composite one foreground with various background images by alpha

blending according to Eq. (1) to generate large-scale synthetic data. The background images are usually choosing from existing benchmarks for image classification and detection, such as MS COCO [14] and PASCAL VOC [15]. However, these background images are in low-resolution and may contain salient objects. In this paper, we point out that the training images following the above route have a significant domain gap with those natural images due to the *composition artifacts*, attributing to the resolution, sharpness, noise, and illumination discrepancies between foreground and background images. The artifacts serve as cheap features to distinguish foreground from background and will mislead the models during training, resulting in overfitted models with poor generalization on natural images.

To address the above issues in animal image matting, we study the distinct roles of semantics and details for animal image matting and explore the idea of decomposing the task into two parallel sub-tasks, semantic segmentation and details matting. Specifically, we propose a novel end-to-end matting model named Glance and Focus Matting network (GFM). It consists of a shared encoder and two separate decoders to learn both tasks in a collaborative manner for animal matting, which is trained end-to-end in a single stage. Moreover, we also explore different data representation formats in the global decoder and gain useful empirical insights into the semantic-transition representation. As shown in Figure 1(a)(iii), compared with previous SOTA methods, GFM is a unified model that models both sub-tasks explicitly and collaboratively in a single network.

Besides, we make the first attempt to establish a large-scale dataset for animal matting, i.e., AM-2k, which con-

tains 2,000 high-resolution *natural* animal images from 20 categories along with manually carefully labeled fine alpha mattes. As shown in (iii) of Figure 1(b) ORI-Track, compared to the datasets in previous work [1], [9], [11] as shown in (i) and (ii) which only provide foreground images or low-resolution inaccurate alpha mattes, AM-2k includes all the original natural images and high-resolution high-quality alpha mattes (more than 1080 pixel in the shorter side), which are beneficial to train models with better generalization on natural animal images. Besides, AM-2k also suggests several new research problems which will be discussed later.

Furthermore, we investigate the domain gap systematically and carry out comprehensive empirical analyses of the composition pipeline in image matting. We identify several kinds of discrepancies that lead to the domain gap and point out possible solutions to them. We then design a novel composition route names RSSN that can significantly reduce the domain gap arisen from the discrepancies of resolution, sharpness, noise, etc. Along with this, as shown in (ii) of Figure 1(b) COMP-Track, we propose a large-scale high-resolution clean background dataset (BG-20k) without salient foreground objects, which can be used in generating high-resolution composite images. Extensive experiments demonstrate that the proposed composition route along with BG-20k can reduce the generalization error by 60% and achieve comparable performance as the model trained using original natural images. It opens an avenue for composition-based image matting since obtaining foreground images and alpha mattes are much easier than those from original natural images by leveraging chroma keying.

The contributions of this paper are four-fold<sup>1</sup>:

- We propose a novel model named GFM for end-to-end natural animal image matting, which simultaneously generates global semantic segmentation and local alpha matte without any priors as input but a single image.
- We construct the first natural animal image matting dataset AM-2k, which benefits training a better model with good generalization by its large scale, diverse categories, and high-quality annotations.
- We design a novel composition route RSSN to reduce various kinds of discrepancies and propose a large-scale high-resolution background dataset BG-20k to serve as better candidates for generating high-quality composite images.
- Extensive experiments on AM-2k and BG-20k demonstrate that GFM outperforms state-of-the-art matting models and can be a strong baseline for future research. Moreover, the proposed composition route demonstrates its value by reducing the generalization error by a large margin.

## 2 RELATED WORK

**Image Matting** Most classical image matting methods are trimap-based [2], [16], [17], [18], [19]. They sample or propagate foreground and background labels to the unknown areas based on local smoothness assumptions. Recently, CNN-based methods improve them by learning discriminative features rather than relying on hand-crafted low-level color features [1], [20], [21], [22], [23]. Deep Matting [1]

employed an encoder-decoder structure to extract high-level contextual features. IndexNet [20] focused on boundary recovery by learning the activation indices during down-sampling. However, trimap-based methods require user interaction, so are not likely to be deployed in automatic applications. Recently, Chen et al. [7] proposed an end-to-end model that first predicted the trimap then carried out matting. Zhang et al. [8] also devised a two-stage model that first segmented the foreground/background and then refined them with a fusion net. Both methods separate the process of segmentation and matting in different stages, which may generate erroneous segmentation results that mislead the matting step. Qiao et al. [9] employed spatial and channel-wise attention to integrate appearance cues and pyramidal features while predicting, however, the distinct appearance and semantics of foreground/background areas and transition areas bring a lot of burden to a single-stage network and limit the quality of alpha matte prediction. Liu et al. [10] proposed a network to perform human matting by predicting the coarse mask first, then adopted a refinement network to predict a more detailed one. Despite the necessity of stage-wise training and testing, a coarse mask is not enough for guiding the network to refine the detail since the transition areas are not defined explicitly.

For animal image matting, the above issue becomes even worse since the appearance diversity of shape, size, texture among different categories of animals as well as the protective coloration of animals make it more challenging to recognize foreground animals or distinguish their fur details from background context. In contrast to previous methods, we devise a novel end-to-end matting model via multi-task learning, which addresses the segmentation and matting tasks simultaneously. It can learn both high-level semantic features and low-level structural features in a shared encoder, benefiting the subsequent segmentation and matting decoders collaboratively. One close related work with ours is AdaMatting [22], which also has a structure of a shared encoder and two decoders. There are several significant differences: 1) AdaMatting requires a coarse trimap as an extra input while our GFM model only takes a single image as input without any priors; 2) the trimap branch in AdaMatting aims to refine the input trimap, which is much easier than generating a global representation in our case because the initial trimap actually serves as an attention mask for learning semantical features; 3) both the encoder and decoder structures of GFM are specifically designed for end-to-end matting, which differs from AdaMatting; and 4) we systematically investigate the semantic-transition representations in the global decoder and gain useful empirical insights.

**Matting Dataset** Existing matting datasets [1], [8], [9], [11], [13] only contain a small number of annotated alpha mattes, *e.g.*, 27 training images and 8 test images in alphamatt [13], 431 training images and 50 test images in Composition-1k [1], and 596 training images and 50 test images in HAttMatting [9]. As for animal matting, there is no large-scale dataset available. Composition-1k only contains 41 and HAttMatting only contains 61 animal images in total, which is far from enough in the deep learning era. We fill this gap by establishing the first natural animal image matting dataset named AM-2k. It contains 2,000

1. The source code, datasets, models, and a video demo will be made publicly available at <https://github.com/JizhiziLi/animal-matting>

high-resolution natural animal images from 20 categories. We manually annotate the alpha matte and category label for each image. In contrast to previous datasets that only provide the foregrounds or composite images, we provide the original natural images. We empirically demonstrate that the model trained on AM-2k has a better generalization ability on natural animal images than the one trained on composite images.

**Image Composition.** As the inverse problem of image matting and the typical way of generating synthetic dataset, image composition plays an important role in image editing. Researchers have been dedicated to improve the reality of composite images from the perspective of color, lighting, texture compatibility and geometric consistency in the past years [24], [25], [26], [27]. Xue et al. [24] conducted experiments to evaluate how the image statistical measure including luminance, color temperature, saturation, local contrast, and hue determine the realism of a composite. Tsai et al. [25] proposed an end-to-end deep convolutional neural network to adjust the appearance of the foreground and background to be more compatible. Chen et al. [26] proposed a generative adversarial network (GAN) architecture to learn geometrically and color consistent in the composites. Cong et al. [27] contributed a large-scale image harmonization dataset and a network using a novel domain verification discriminator to reduce the inconsistency of foreground and background. Although they all done a good job in harmonizing the composites to be more realistic, the domain gap still exists when fitting the synthesis data into the matting model, the reason is a subjective agreed standard of harmonization by a human is not equivalent to a good training candidate for a machine learning model. In this paper, instead of working on generating consistent look composite images, we focus on generating composite images that can be used to reduce the generalization error on natural images of matting models.

**Domain Adaptation** Due to the tedious labor required to collect and annotate large-scale natural images from the real-world scenarios for different computer vision tasks such as image matting [1], [28], crowd counting [29], object detection [30], and semantic segmentation [31], leveraging synthetic data to increase the volume of training set for deep learning method becomes gradually prevalent, e.g., obtaining synthetic images from 3D virtual game engine for semantic segmentation [32]. However, the domain gap between the synthetic images and real-world images degrades the generalization ability of deep models.

To address this issue, many efforts have been made in the domain adaptation community. For example, Wang et al. [29] proposed an SSIM Embedding (SE) Cycle GAN architecture to transform the synthetic domain to real-world domain. Dwibedi et al. [30] adopted Poisson blending [33] and Gaussian noise to the synthetic data to smooth the boundary artifacts. Sankaranarayanan et al. [32] utilized an approach based on GAN to bring the embedding of synthetic data closer in the learned feature space. Mayer et al. [34] evaluated the importance of object shape, motion type, camera lens distortion, and Bayer artifact in improving the performance of optical flow estimation tasks.

However, the domain gap between synthetic images and real-world natural images in image matting attributes to

different types of discrepancies between the foreground and background images introduced during the specific alpha-composition process, e.g., resolution, sharpness, noise, etc. Sengupta et al. [28] reduced the domain gap by augmenting the dataset and devising a context switching block and self-supervised train the network on real unlabeled input images. In this paper, we systematically investigate the discrepancies that lead to the domain gap and design a novel composition route that can significantly reduce it. As a result, we successfully reduce the generalization error by a large margin for different models trained on images generated by the proposed composition route.

### 3 GFM: GLANCE AND FOCUS MATTING NETWORK

When tackling the animal image matting problem, we humans first glance at the image to quickly recognize the salient rough foreground or background areas and then focus on the transition areas to distinguish details from the background. It can be formulated as a rough segmentation stage and a matting stage roughly. Note that these two stages may be intertwined that there will be feedback from the second stage to correct the erroneous decision at the first stage, for example, in some ambiguous areas due to the protective coloration of animals or occlusions. To mimic the human experience and empower the matting model with proper abilities at both stages, it is reasonable to integrate them into a single model and explicitly model the collaboration. To this end, we propose a novel Glance and Focus Matting network for end-to-end natural animal image matting.

#### 3.1 Shared Encoder

As shown in Figure 2, GFM has an encoder-decoder structure, where the encoder is shared by two subsequent decoders. The encoder takes a single image as input and processes it through five blocks  $E_0 \sim E_4$ , where each reduces the resolution by half. We adopt the ResNet-34 [35] or DenseNet-121 [36] pre-trained on the ImageNet training set as our backbone encoder. Specifically, for DenseNet-121, we add a convolution layer to reduce the output feature channels to 512.

#### 3.2 Glance Decoder (GD)

The glance decoder aims to recognize the easy semantic parts and leave the others as unknown areas. To this end, the decoder should have a large receptive field to learn high-level semantics. As shown in Figure 2, we symmetrically stack five blocks  $D_4^G \sim D_0^G$  as the decoder, each of which consists of three sequential  $3 \times 3$  convolutional layers and an upsampling layer. To enlarge the receptive field further, we add a *pyramid pooling module* (PPM) [37], [38] after  $E_4$  to extract global context, which is connected to each decoder block  $D_i^G$  by element-wise summation. We adopt a sigmoid activation function after the decoder output.

**Loss Function** The training loss for glance decoder is a cross-entropy loss, denoted  $L_{CE}$  in Eq. (2).

$$L_{CE} = - \sum_{c=1}^C G_g^c \log(G_p^c), \quad (2)$$

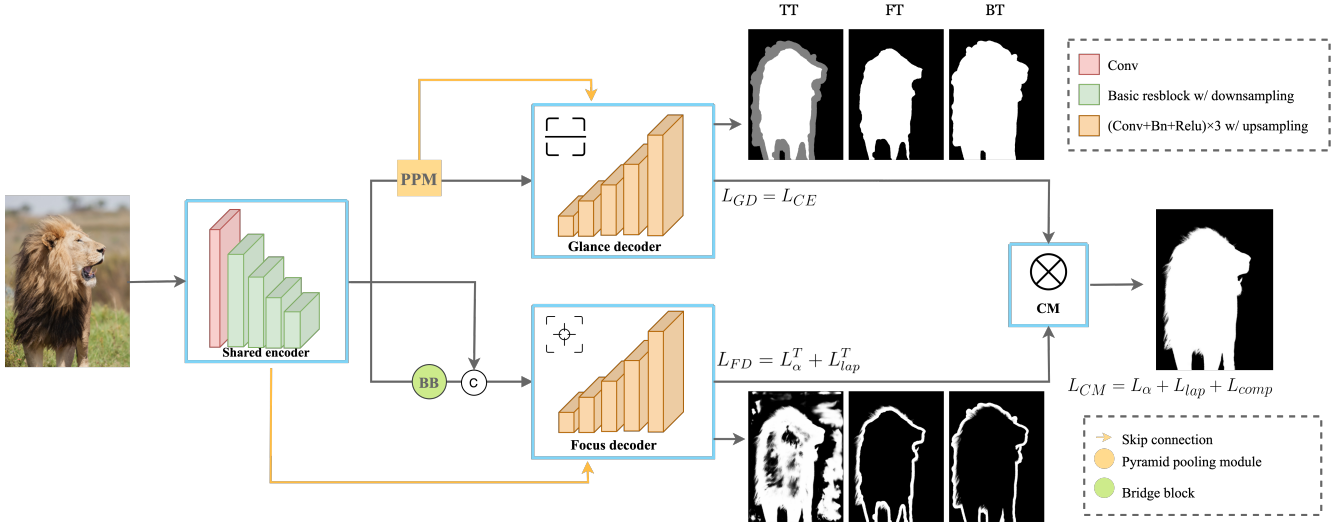


Fig. 2. Diagram of the proposed Glance and Focus Matting (GFM) network, consists of a shared encoder and two separate decoders responsible for whole image rough segmentation and transition area's details matting.

where  $G_p^c \in [0, 1]$  is the predicted probability for  $c$ th class,  $G_g^c \in \{0, 1\}$  is the ground truth label. The output of GD is a two- or three-channel ( $C = 2$  or  $3$ ) class probability map depends on the semantic-transition representation, which will be detailed in Section 3.4.

### 3.3 Focus Decoder (FD)

As shown in Figure 2, FD has the same basic structure as GD, i.e., symmetrically stacked five blocks  $D_4^F \sim D_0^F$ . Different from GD, which aims to do roughly semantic segmentation, FD aims to extract details in the transition areas where low-level structural features are very useful. Therefore, we use a *bridge block* (BB) [39] instead of the PPM after  $E_4$  to leverage local context in different receptive fields. Specifically, it consists of three dilated convolutional layers. The features from both  $E_4$  and BB are concatenated and fed into  $D_4^F$ . We follow the U-net [40] style and add a shortcut between each encoder block  $E_i$  and the decoder block  $D_i^F$  to preserve fine details.

**Loss Function** The training loss for FD ( $L_{FD}$ ) is consist of an alpha-prediction loss  $L_\alpha^T$  and a Laplacian loss  $L_{lap}^T$  in the unknown transition areas [1], i.e.,

$$L_{FD} = L_\alpha^T + L_{lap}^T \quad (3)$$

Following [1], the alpha loss  $L_\alpha^T$  is calculated as absolute difference between ground truth  $\alpha$  and predicted alpha matte  $\alpha^F$  in the unknown transition region. It is defined as follows:

$$L_\alpha^T = \frac{\sum_i \sqrt{((\alpha_i - \alpha_i^F) \times W_i^T)^2 + \varepsilon^2}}{\sum_i W_i^T}, \quad (4)$$

where  $i$  denotes pixel index,  $W_i^T \in \{0, 1\}$  denotes whether pixel  $i$  belongs to the transition region or not. We add  $\varepsilon = 10^{-6}$  for computational stability.

Following [21], the Laplacian loss  $L_{lap}^T$  is defined as the  $L1$  distance between the Laplacian pyramid of ground truth

and that of prediction. We use five levels in the Laplacian pyramid.  $L_{lap}^T$  can be formulated as follows:

$$L_{lap}^T = \sum_i W_i^T \sum_{k=1}^5 \|(Lap^k(\alpha_i) - Lap^k(\alpha_i^F))\|_1, \quad (5)$$

where  $Lap^k$  denotes the  $k$ th level of the Laplacian pyramid.

### 3.4 RoSTa: Representation of Semantic and Transition Area

To investigate the impact of the representation format of the supervisory signal in our GFM, we adopt three kinds of Representations of Semantic and Transition areas (RoSTa) as bridge to link GD and FD.

- **GFM-TT** We use the classical 3-class trimap  $T$  as the supervisory signal for GD, which is generated by dilation and erosion from ground truth alpha matte with a kernel size of 25. We use the ground truth alpha matte  $\alpha$  in the unknown transition areas as the supervisory signal for FD.
- **GFM-FT** We use the 2-class foreground segmentation mask  $F$  as the supervisory signal for GD, which is generated by the erosion of ground truth alpha matte with a kernel size of 50 to ensure the left foreground part is correctly labeled. In this case, the area of  $\mathcal{I}(\alpha > 0) - F$  is treated as the transition area, where  $\mathcal{I}(\cdot)$  denotes the indicator function. We use the ground truth alpha matte  $\alpha$  in the transition area as the supervisory signal for FD.
- **GFM-BT** We use the 2-class background segmentation mask  $B$  as the supervisory signal for glance decoder, which is generated by dilation of ground truth alpha matte with kernel size as 50 to ensure the left background part is correctly labeled. In this case, the area of  $B - \mathcal{I}(\alpha > 0)$  is treated as the transition area. We use the ground truth alpha matte  $\alpha$  in the transition area as the supervisory signal for FD.

### 3.5 Collaborative Matting (CM)

As shown in Figure 2, CM merges the predictions from GD and FD to generate the final alpha prediction. Specifically, CM follows different rules when using different RoSTa as described in Section 3.4. In GFM-TT, CM replaces the transition area of the prediction of GD with the prediction of FD. In GFM-FT, CM adds the predictions from GD and FD to generate the final alpha matte. In GFM-BT, CM subtracts the prediction of FD from the prediction of GD as the final alpha matte. In this way, GD takes charge of recognizing rough foreground and background by learning global semantic features, and FD is responsible for matting details in the unknown areas by learning local structural features. Such task decomposition and specifically designed parallel decoders make the model simpler than the two-stage ones in [7], [8]. Besides, both decoders are trained simultaneously that the loss can be backpropagated to each of them via the merging node. In this way, our model enables interaction between both decoders that the erroneous prediction can be corrected in time by the responsible branch. Obviously, it is expected to be more effective than the two-stage framework, where the erroneous segmentation in the first stage could not be corrected by the subsequent one and thus mislead it.

**Loss Function** The training loss for collaborative matting ( $L_{CM}$ ) consists of an alpha-prediction loss  $L_\alpha$ , a Laplacian loss  $L_{lap}$ , and a composition loss  $L_{comp}$ , i.e.,

$$L_{CM} = L_\alpha + L_{lap} + L_{comp}. \quad (6)$$

Here  $L_\alpha$  and  $L_{lap}$  are calculated according to Eq. (4) and Eq. (5) but in the whole alpha matte. Following [1], the composition loss ( $L_{comp}$ ) is calculated as the absolute difference between the composite images based on the ground truth alpha and the predicted alpha matte by referring to [2]. It can be defined as follows:

$$L_{comp} = \frac{\sum_i \sqrt{(C(\alpha_i) - C(\alpha_i^{CM}))^2 + \varepsilon^2}}{N}, \quad (7)$$

where  $C(\cdot)$  denotes the composited image accordingly,  $\alpha^{CM}$  is the predicted alpha matte by CM,  $N$  denotes the number of pixels in the alpha matte.

To sum up, the final loss used during training is calculated as the linear combination of  $L_{CE}$ ,  $L_{FD}$  and  $L_{CM}$ , i.e.,

$$L = \lambda_1 L_{CE} + \lambda_2 L_{FD} + \lambda_3 L_{CM}, \quad (8)$$

where  $\lambda_1 \sim \lambda_3$  are loss weights to balance different losses. They are set to 0.25 in this paper.

## 4 RSSN: A NOVEL COMPOSITION ROUTE

Since labeling alpha matte of real-world natural images is very laborious and costly, a common practice is to generate large-scale composition images from a few of foreground images and the paired alpha mattes [1]. The prevalent matting composition route is to paste one foreground with various background images by alpha blending according to Eq. (1). However, since the foreground and background images are usually sampled from different distributions, there will be a lot of *composition artifacts* in the composite images, which bring in a large domain gap between the composition images and natural ones. The composition artifacts may

mislead the model by serving as cheap features, resulting in overfitting on the composite images and producing large generalizing errors on natural images.

In this section, we systematically analyze the factors that cause the *composition artifacts* including Resolution discrepancy, Semantic ambiguity, Sharpness discrepancy, and Noise discrepancy. To address these issues, we propose a new composition route named RSSN and a large-scale high-resolution background dataset named BG-20k.

### 4.1 Resolution Discrepancy and Semantic Ambiguity

In the literature of image matting, the background images used for composition are usually chosen from existing benchmarks for image classification and detection, such as MS COCO [14] and PASCAL VOC [15]. However, these background images are in low-resolution and may contain salient objects, causing the following two types of discrepancies.

- 1) **Resolution Discrepancy:** A typical image in MS COCO [14] or Pascal VOC [15] has a resolution about  $389 \times 466$ , which is much smaller compared to the high-resolution foreground images in matting dataset such as Composition-1k [1]. The resolution discrepancy between foreground and background images will result in obvious artifacts as shown in Figure 3(b).
- 2) **Semantic ambiguity:** Images in MS COCO [14] and Pascal VOC [15] are collected for classification and object detection tasks, which usually contain salient objects from different categories, including various animals. Directly pasting the foreground image with such background images will result in semantic ambiguity for end-to-end image matting. For example, as shown in Figure 3(b), there is a dog in the background which is beside the leopard in the composite image. Training with such images will mislead the model to ignore the background animal, i.e., probably learning few about semantics but more about discrepancies.

To address these issues, we propose a large-scale high-resolution dataset named BG-20k to serve as good background candidates for composition. We only selected those images whose shortest side has at least 1080 pixels to reduce the resolution discrepancy. Moreover, we removed those images containing salient objects to eliminate semantic ambiguity. The details of constructing BG-20k are presented as follows.

- 1) We collected 50k high-resolution (HD) images using the keywords such as *HD background*, *HD view*, *HD scene*, *HD wallpaper*, *abstract painting*, *interior design*, *art*, *landscape*, *nature*, *street*, *city*, *mountain*, *sea*, *urban*, *suburb* from websites with open licenses<sup>2</sup>, removed those images whose shortest side has less than 1080 pixels and resized the left images to have 1080 pixels at the shortest side while keeping the original aspect ratio. The average resolution of images in BG-20k is  $1180 \times 1539$ ;

2. <https://unsplash.com/> and <https://www.pexels.com/>



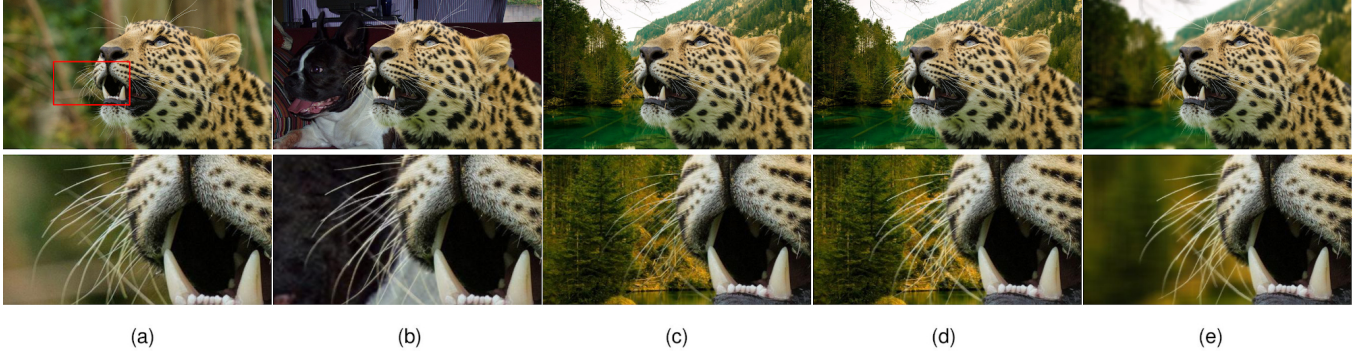


Fig. 3. Comparison of different image composition methods. (a) Original natural image. (b) Composite with background from MS COCO [14] with foreground computed by [2]. (c) Composite with background from our proposed BG-20k by alpha blending of original image directly. (d) Composite with background from our proposed BG-20k with foreground computed by [2]. (e) Composite with large-aperture effect.



Fig. 4. Some examples from our BG-20k dataset.

- 2) We removed duplicate images by a deep matching model [41]. We adopted YOLO-v3 [42] to detect salient objects and then manually double-checked to make sure each image has no salient objects. In this way, we built BG-20k containing 20,000 high-resolution clean images;
- 3) We split BG-20k into a disjoint training set (15k) and validation set (5k).

An composition example using the background image from BG-20k is shown in Figure 3(c) and Figure 3(d). In (c), we use the foreground image computed by multiplying ground truth alpha matte with the original image for alpha blending, in (d), we use the foreground image computed by referring to the method in [2] for alpha blending. As can be seen, there are obvious color artifacts in (c) that blends both colors of foreground and background in the fine details. The composite image in (d) is much more realistic than that in (c). Therefore, we adopt the method in [2] for computing foreground images in our composition route. More examples of BG-20k are presented in Figure 4 and the supplementary video to show its diversity.

## 4.2 Sharpness Discrepancy

In photography, it is usually to use a large aperture and focal length to capture a sharp and salient foreground image within the shallow depth-of-field, thus highlighting it from the background context, which is usually blurred due to the out-of-focus effect. An example is shown in Figure 3(a), where the leopard is the center of interest and the background is blurred. Previous composition methods

dismiss this effect, producing a domain gap of sharpness discrepancy between the composite images and natural photos. Since we target the animal matting task, where the animals are usually salient in the images, thereby we investigate this effect in our composition route. Specifically, we simulate it by adopting the averaging filter in OpenCV with a kernel size chosen from 20, 30, 40, 50, 60 randomly to blur the background images. Since some natural photos may not have blurred backgrounds, we only use this technique in our composition route with a probability of 0.5. An example is shown in Figure 3(e), where the background is chosen from BG-20k and blurred using the averaging filter. As can be seen, it has a similar style to the original image in (a).

## 4.3 Noise Discrepancy

Since the foreground and background come from different image sources, they may contain different noise distributions. This is another type of discrepancy, which will mislead the model to search noise cues during training, resulting in overfitting. To address this discrepancy, we adopt BM3D [43] to remove noise in both foreground and background images in RSSN. Furthermore, we add Gaussian noise with a standard deviation of 10 to the composite image such that the noise distributions in both foreground and background areas are the same. We find that it is effective in improving the generalization ability of trained models.

## 4.4 the Proposed Composition Route

We conclude the pipeline of our proposed composition route RSSN in Pipeline 1. The input of the pipeline is the matting dataset, e.g. our proposed AM-2k as will be introduced in Section 5, DIM [1], or DAPM [11] and the proposed background image set BG-20k. If the matting dataset provides original images, e.g. AM-2K, DAPM [11], we compute the foreground from the original image given the alpha matte by referring to [2]. We random sample  $K$  background candidates from BG-20k for each foreground for data augmentation. We set  $K = 5$  in our experiments. For each foreground image and background image, we carried out the denoising step with a probability of 0.5. To simulate the effect of large-aperture, we carried out the blur step on the background image with a probability of 0.5, where the blur

kernel size was randomly sampled from  $\{20, 30, 40, 50, 60\}$ . We then generated the composite image according to the alpha-blending equation Eq. (1). Finally, with a probability of 0.5, we added Gaussian noise to the composite image to ensure the foreground and background areas have the same noise distribution. To this end, we generate a composite image set that has reduced many kinds of discrepancies, thereby narrowing the domain gap with natural images.

---

**Pipeline 1: the Proposed Composition Route: RSSN**


---

**Input:** The matting dataset  $M$  containing  $|M|$  images and the background image set BG-20k

**Output:** The composite image set  $C$

---

```

1: for each  $i \in [1, |M|]$  do
2:   if there are original images in  $M$ , e.g. AM-2k, then
3:     Sample an original image  $I_i \in M$ 
4:     Sample the paired alpha matte  $\alpha_i \in M$ 
5:     Compute the foreground  $F_i$  given  $(I_i, \alpha_i)$  [2]
6:   else
7:     Sample a foreground image  $F_i \in M$ 
8:     Sample the paired alpha matte  $\alpha_i \in M$ 
9:   end if
10:  for each  $k \in [1, K]$  do
11:    Sample a background candidate  $B_{ik} \in \text{BG-20k}$ 
12:    if  $\text{random}() < 0.5$  then
13:       $F_i = \text{Denoise}(F_i)$  //denoising by BM3D [43]
14:       $B_{ik} = \text{Denoise}(B_{ik})$ 
15:    end if
16:    if  $\text{random}() < 0.5$  then
17:      Sample a blur kernel size  $r \in \{20, 30, 40, 50, 60\}$ 
18:       $B_{ik} = \text{Blur}(B_{ik}, r)$  // the averaging filter
19:    end if
20:    Alpha blending:  $C_{ik} = F_i \times \alpha_i + B_{ik} \times (1 - \alpha_i)$ 
21:    if  $\text{random}() < 0.5$  then
22:       $C_{ik} = \text{AddGaussianNoise}(C_{ik})$ 
23:    end if
24:  end for
25: end for

```

---

## 5 AM-2K: ANIMAL MATTING DATASET

In this section, we present the details of our AM-2k dataset, including the process of collection and labeling, a brief comparison with other matting datasets, the dataset partition, and benchmark tracks.

### 5.1 Dataset Collection and Labeling

The collection and labeling process of AM-2k are as follows:

- 1) collect about 5,000 animal-related images from websites with open licenses as in Section 4.1, make sure they are free to use and their shortest sides have more than 1080 pixels;
- 2) retain images containing salient animals of clear appearance and remove duplicate images by a deep matching model [41];
- 3) resize the retained images to have 1080 pixels at the shortest side while keeping the original aspect ratio;

- 4) manually annotate the category label for each image and the alpha matte using open-source image editing software, e.g. Adobe Photoshop, GIMP, etc.

After the above process, we build our AM-2k dataset which contains 2,000 animal images in total from 20 categories evenly. All the categories are listed as follows in alphabetical order: *alpaca, antelope, bear, camel, cat, cattle, deer, dog, elephant, giraffe, horse, kangaroo, leopard, lion, monkey, rabbit, rhinoceros, sheep, tiger, zebra*. We present some examples from our AM-2k dataset in Figure 5, where the original images and the corresponding alpha mattes are displayed. More examples can be found in the supplementary video.

We make a brief comparison between our AM-2k dataset and other representative matting datasets in the literature from the perspective of availability of original images (AOI), dataset volume, average resolution, and the volume of animal images. The results are summarized in Table 1. Compared with DAPM [11] and LF [8], images and alpha mattes in our AM-2k have higher resolution, which is very important for high-definition image matting, e.g., extracting fine details in images. Besides, AM-2k is specifically constructed for animal matting while other datasets only contain a few or no animal images. Compared to Comp-1k [1], LF [8], and HAtt [9], AM-2k has more images and also provides the original images, where the others only provide the foreground images. As we will demonstrate in the experiment part, the common practice that training on composite images based on the foregrounds will result in a model with poor generalization on natural images, since it may bias towards the composition artifacts. On the contrary, the model trained on AM-2k has no such a drawback since we provide the original *natural* images.

TABLE 1  
Comparison between AM-2k and existing matting datasets.

Dataset	AOI	Volume	Resolution	Animal
DAPM [11]	✓	2,000	800 × 600	0
Comp-1k [1]	×	481	1,083 × 1,298	41
LF [8]	×	257	756 × 553	0
HAtt [9]	×	646	1730 × 1572	61
AM-2k	✓	2,000	1,196 × 1,470	2,000

### 5.2 Dataset Partition and Benchmark Tracks

After constructing AM-2k, we then partition it into disjoint training and validation sets and set up two evaluation tracks for different purposes. Details are given below:

- 1) **ORI-Track** (Original Images Based Track) is set to perform end-to-end matting tasks on the original natural images. We randomly select 90 images in each category to form the training set while using the left 10 images in each category to form the validation set. We also reserve another 500 images from the other five categories of animals that are disjoint from the training and validation sets, serving as the test set. The ORI-Track is the primary benchmark track.
- 2) **COMP-Track** (Composite Images Based Track) is set to carry out domain adaptation studies for image matting. As discussed before, the composite images





Fig. 5. Some examples from our AM-2k dataset. The alpha matte is displayed beside the original image.

have a large domain gap with natural images due to the composition artifacts. If we can reduce the domain gap and learn a domain-invariant feature representation, we can obtain a model with better generalization. To this end, we set up this track by making the first attempt to this research direction. Specifically, we construct the composite training set by alpha-blending each foreground with five background images from the COCO dataset [14] (denote as COMP-COCO) and our BG-20k dataset (denote as COMP-BG20K), or adopting the composition route RSSN proposed in Section 4.4 based on our BG-20K (denote as COMP-RSSN). Moreover, unlike previous benchmarks that evaluate matting methods on composite images [1], [8], [9], we evaluate matting methods on natural images of the validation set in the ORI-Track to validate their generalization ability.

## 6 EMPIRICAL STUDIES

### 6.1 Experiment Settings

**Datasets.** Experiments were carried out on two tracks of our AM-2k dataset: 1) to compare our proposed method with state-of-the-art (SOTA) methods, we trained and evaluated them on the ORI-Track; 2) to evaluate the side effect of domain gap caused by composition and the proposed composition route, we trained and evaluated GFM and SOTA methods on the COMP-Track, i.e., COMP-COCO, COMP-BG20k, and COMP-RSSN, respectively.

**Evaluation Metrics.** Following the common practice in [1], [8], [13], we used the mean squared error (MSE), the sum of absolute differences (SAD), gradient (Grad.), and connectivity (Conn.) as the major metrics to evaluate the quality of alpha matte predictions. Note that the MSE and SAD metrics evaluate the quantitative difference between the prediction and ground truth alpha matte, while the gradient and connectivity metrics favor clear details. Besides, we also use some auxiliary metrics such as Mean Absolute Difference (MAD), SAD-TRAN (SAD in the transition areas), SAD-FG (SAD in the foreground areas), and SAD-BG (SAD in the background areas) to comprehensively evaluate the quality of alpha matte prediction. While MAD evaluates the average quantitative difference regardless of the image size, SAD-TRAN, SAD-FG, and SAD-BG evaluate SAD in different semantic areas, respectively. In addition, we also compared the model complexity of different methods in terms of

the number of parameters, computational complexity, and inference time.

**Implementation Details** During training, we used multi-scale augmentation similar to [1]. Specifically, we cropped each of the selected images with size from  $\{640 \times 640, 960 \times 960, 1280 \times 1280\}$  randomly, resized the cropped image to  $320 \times 320$ , and randomly flipped it with a probability of 0.5. The encoder of GFM was initialized with the ResNet-34 [35] or DenseNet-121 [36] pre-trained on the ImageNet dataset. GFM was trained on two NVIDIA Tesla V100 GPUs. The batch size was 4 for DenseNet-121 [36] and 32 for ResNet-34 [35]. For COMP-Track, we composite five training images by using five different backgrounds for each foreground on-the-fly during training. It took about two days to train GFM for 500 epochs on ORI-Track and 100 epochs for COMP-Track. The learning rate was fixed to  $1 \times 10^{-4}$  for the ORI-Track and  $1 \times 10^{-5}$  for the COMP-Track.

For baseline methods LF [8] and SSS [12], we used the official codes released by authors. For SHM [7], HAtt [9] and SHMC [10] with no public codes, we re-implemented them according to the papers. For SHMC [10] which does not specify the backbone network, we used ResNet-34 [35] for a fair comparison. These models were trained using the training set on ORI-Track or COMP-Track.

### 6.2 Quantitative and Subjective Evaluation

**Results on the ORI-Track.** We benchmarked several SOTA methods [7], [8], [9], [10], [12] on the ORI-Track of AM-2k. The results are summarized in the top of Table 2. GFM-TT, GFM-FT, and GFM-BT denote the proposed GFM model with different RoSTa as described in Section 3.4. (*d*) stands for using DenseNet-121 [36] as the backbone encoder while (*r*) stands for using ResNet-34 [35] as the backbone encoder. There are several empirical findings from Table 2.

**First**, SSS [12] achieved the worst performance with a large foreground SAD error of 401.66 compare with others, the reason can be twofold: 1) they adopt the pre-trained Deeplab-ResNet-101 [44] model as the semantic feature extractor to calculate affinities. The pre-trained model may generate limited representative features on our high-resolution animal matting dataset which degrade the performance; and 2) this method aims to extract all the semantic regions in the image while other matting methods are trained to extract only the salient animal foreground. **Second**, SHMC using global guidance [10] and stage-wise method LF [8] perform better than SSS [12] in all evaluation metrics. However, the SAD errors in the transition area

TABLE 2  
Results on AM-2k's ORI-Track, COMP-Track. (*d*) stands for DenseNet-121 [36] backbone, (*r*) stands for ResNet-34 [35] backbone. Representations of *TT*, *FT* and *BT* can refer to Section 3.4.

Track	ORI										
Method	SHM [7]	LF [8]	SSS [12]	HAtt [9]	SHMC [10]	GFM-TT( <i>d</i> )	GFM-FT( <i>d</i> )	GFM-BT( <i>d</i> )	GFM-TT( <i>r</i> )	GFM-FT( <i>r</i> )	GFM-BT( <i>r</i> )
SAD	17.81	36.12	552.88	28.01	61.50	<b>10.27</b>	12.74	12.74	10.89	12.58	12.61
MSE	0.0068	0.0116	0.2742	0.0055	0.0270	<b>0.0027</b>	0.0038	0.0030	0.0029	0.0037	0.0028
MAD	0.0102	0.0210	0.3225	0.0161	0.0356	<b>0.0060</b>	0.0075	0.0075	0.0064	0.0073	0.0074
Grad.	12.54	21.06	60.81	18.29	37.00	<b>8.80</b>	9.98	9.13	10.00	10.33	9.27
Conn.	17.02	33.62	555.97	17.76	60.94	<b>9.37</b>	11.78	10.07	9.99	11.65	9.77
SAD-TRAN	10.26	19.68	88.23	13.36	35.23	<b>8.45</b>	9.66	8.67	9.15	9.34	8.77
SAD-FG	0.60	3.79	401.66	1.36	10.93	<b>0.57</b>	1.47	3.07	0.77	1.31	2.84
SAD-BG	6.95	12.55	62.99	13.29	15.34	1.26	1.61	1.00	<b>0.96</b>	1.93	1.00
Track	COMP-COCO			COMP-BG20K			COMP-RSSN				
Method	SHM [7]	GFM-TT( <i>d</i> )	GFM-TT( <i>r</i> )	SHM [7]	GFM-TT( <i>d</i> )	GFM-TT( <i>r</i> )	SHM [7]	GFM-TT( <i>d</i> )	GFM-FT( <i>d</i> )	GFM-BT( <i>d</i> )	GFM-TT( <i>r</i> )
SAD	182.70	46.16	30.05	52.36	25.19	16.44	23.94	19.19	20.07	22.82	<b>15.88</b>
MSE	0.1017	0.0223	0.0129	0.02680	0.0104	0.0053	0.0099	0.0069	0.0072	0.0078	<b>0.0049</b>
MAD	0.1061	0.0273	0.0176	0.03054	0.0146	0.0096	0.0137	0.0112	0.0118	0.0133	<b>0.0092</b>
Grad.	64.74	20.75	17.22	22.87	15.04	14.64	17.66	13.37	12.53	<b>12.49</b>	14.04
Conn.	182.05	45.39	29.19	51.76	24.31	15.57	23.29	18.31	19.08	19.96	<b>15.02</b>
SAD-TRAN	25.01	17.10	15.21	15.32	13.35	12.36	12.63	12.10	12.12	12.06	<b>12.03</b>
SAD-FG	23.26	8.71	4.74	3.52	3.79	1.46	4.56	4.37	3.47	5.20	<b>1.15</b>
SAD-BG	134.43	20.36	10.1	33.52	8.05	2.62	6.74	2.72	4.48	5.56	<b>2.71</b>

dominate the total errors, which is 35.23 and 19.68 respectively. The reason is that both of them have not explicitly define the transition area, thereby the matting network has limited ability to distinguish the details in the transition area when it needs segment foreground and background areas using the same network at the same time. It can also be confirmed by the scores of Grad. and Conn. **Third**, HAtt [9] performs better than SHMC [10] and LF [8] in terms of SAD error in the transition area and foreground area because the attention module it adopted can provide better global appearance filtration. However, using a single network to model both the foreground and background areas and the transition areas of plentiful details makes it hard to powerful representative features for both areas, resulting in large SAD errors especially in the background areas as well as large Grad. and Conn. errors.

**Fourth**, SHM [7] performs the best among all the SOTA methods. It reduces the SAD error in the transition area from 13.36 to 10.26 and the SAD error in the background area from 13.29 to 6.95 compared with HAtt [9]. We believe the improvement credits to the explicit definition of RoSTa and the PSPNet [37] used in the first stage which has a good semantic segmentation capability. However, SHM [7] still has large error in the background area due to its stage-wise pipeline, which will accumulate the segmentation error into the matting network. **Last**, compare with all the SOTA methods, GFM outperforms them in all evaluation metrics, achieving the best performance by simultaneously segmenting the foreground and background and matting on the transition areas, no matter which kind of RoSTa it uses. For example, it achieves the lowest SAD error in different areas, *i.e.* 8.45 v.s. 10.26 in the transition area, 0.57 v.s. 0.60 in the foreground area, and 0.96 v.s. 6.95 in the background area compared with the previous best method SHM [7]. The results of using different RoSTa are comparable, especially for FT and BT, since they both define two classes in the image for segmentation by the Glance Decoder. GFM using TT as RoSTa performs the best due to its explicit definition of the transition area as well as the foreground and

background areas. We also tried two different backbone networks, ResNet-34 [35] and DenseNet-121 [36]. Both of them achieve the best performance compared with other SOTA methods, while DenseNet-121 [36] is marginally better.

The reason of GFM's superiority over other methods can be explained as follows. First, compared with stage-wise methods *e.g.* SHM [7], SSS [12] and LF [8], GFM can be trained in a single stage and the collaboration module acts as an effective gateway to propagate matting errors to the responsible branch adaptively. Second, compared with methods that adopt global guidance *e.g.* HAtt [9] and SHMC [10], GFM explicitly model the end-to-end matting task into two separate but collaborate sub-tasks by two distinct decoders. Moreover, it uses a collaboration module to merge the predictions according to the definition of RoSTa, which explicitly defines the role of each decoder.

From Figure 6, we can find similar observations. SHM [7], LF [8], and SSS [12] fail to segment some foreground parts, implying inferiority of its stage-wise network structure, since they do not distinguish the foreground/background and the transition areas explicitly in the model. It is hard to balance the role of semantic segmentation for the former and matting details for the latter, which requires global semantic and local structural features, respectively. HAtt [9] and SHMC [10] struggle to obtain clear details in the transition areas since the global guidance is helpful for recognizing the semantic areas while being less useful for matting of details. Compared to them, GFM achieves the best results owing to the virtue of a unified model, which deals with the foreground/background and transition areas using separate decoders and optimizes them in a collaborative manner. More results of GFM can be found in the supplementary video.

**Results on the COMP-Track.** We evaluated the best performed SOTA method SHM [7] and our GFM with two different backbones on AM-2k's COMP-Track including COMP-COCO, COMP-BG20K, and COMP-RSSN. The results are summarized in the bottom of Table 2, from which we have several empirical findings. **First**, when training

matting models using images from MS COCO dataset [14] as backgrounds, GFM performs much better than SHM [7], *i.e.* 46.16 and 30.05 v.s. 182.70 in whole image SAD, confirming the superiority of the proposed model over the two-stage one for generalization. **Second**, GFM using ResNet-34 [35] performs better than using DenseNet-121 [36], which is different from the results on the ORI-TRACK. We suspect that DenseNet-121 has a slightly better representation capacity than ResNet-34, thereby it can achieve better results on the ORI-TRACK while being a little overfitting of composite images on the COMP-TRACK. **Third**, when training matting models using background images from the proposed BG-20k dataset, the errors of all the methods are significantly reduced, especially for SHM [7], *i.e.*, from 182.70 to 52.36, which mainly attributes to the reduction of SAD error in the background area, *i.e.*, from 134.43 to 33.52. There is the same trend for GFM(d) and GFM(r) as well. These results confirm the value of our BG-20k, which helps to reduce resolution discrepancy and eliminate semantic ambiguity in the background area. **Fourth**, when training matting models using the proposed composition route, the errors can be reduced further, *i.e.*, from 52.36 to 23.94 for SHM [7], from 25.19 to 19.19 for GFM(d), and from 16.44 to 15.88 for GFM(r). The performance improvement is attributed to the composition techniques in our RSSN: 1) we simulate the large-aperture effect to reduce sharpness discrepancy; and 2) we remove the noise of foreground/background and add noise to the composite image to reduce noise discrepancy. It is noted that the SAD error of SHM [7] has dramatically reduced about 87% from 182.70 to 23.93 when using the proposed RSSN for composition compared with using the traditional composition method based on MS COCO dataset, which is even comparable with the one obtained by training using original images, *i.e.*, 17.81. It demonstrates that the proposed composition route RSSN can significantly *narrow* the domain gap between the composite images and real-world natural images. **Last**, We also conducted experiments by using different RoSTa in GFM(d) on COMP-RSSN, their results have a similar trend to that on the ORI-TRACK.

### 6.3 Model Ensemble and Hybrid-resolution Test

TABLE 3  
Model Ensemble and Hybrid-resolution Test.

Track		Ensemble				
Method		SAD	MSE	MAD	Grad.	Conn.
GFM-ENS(d)		<b>9.21</b>	<b>0.0021</b>	<b>0.0054</b>	<b>8.00</b>	<b>8.16</b>
GFM-ENS(r)		9.92	0.0024	0.0058	8.82	8.92
Track		Hybrid				
$d_1$	$d_2$	SAD	MSE	MAD	Grad.	Conn.
1/2	1/2	12.57	0.0041	0.0074	9.26	11.75
<b>1/3</b>	<b>1/2</b>	<b>10.27</b>	<b>0.0027</b>	<b>0.0060</b>	<b>8.80</b>	<b>9.37</b>
1/3	1/3	11.58	0.0028	0.0067	11.67	10.67
1/4	1/2	13.23	0.0045	0.0078	10.00	12.26
1/4	1/3	14.65	0.0047	0.0086	12.46	13.68
1/4	1/4	17.29	0.0055	0.0102	16.50	16.28

**Model Ensemble** Since we propose three different RoSTa for GFM, it is interesting to investigate their complementary. To this end, we calculated the result by a model ensemble which takes the median of the alpha predictions from three

models as the final prediction. As shown in Table 3, the result of the model ensemble is better than any single one, *i.e.*, 9.21 v.s. 10.27 for GFM-TT(d), 9.92 v.s. 10.89 for GFM-TT(r), confirming the complementarity between different RoSTa.

**Hybrid-resolution Test** For our GFM, we also proposed a hybrid-resolution test strategy to balance GD and FD. Specifically, we first fed a down-sampled image to GFM to get an initial result. Then, we used the full resolution image as input and only used the predicted alpha matte from FD to replace the initial prediction in the transition areas. For simplicity, we denote the down-sampling ratio at each step as  $d_1$  and  $d_2$ , which are subject to  $d_1 \in \{1/2, 1/3, 1/4\}$ ,  $d_2 \in \{1/2, 1/3, 1/4\}$ , and  $d_1 \leq d_2$ . We summarize the results of GFM-TT(d) in Table 3. A smaller  $d_1$  increases the effective receptive field and benefits the Glance Decoder, while a larger  $d_2$  stands for a higher resolution image and benefits the Focus Decoder with clear details. Finally, we set  $d_1 = 1/3$  and  $d_2 = 1/2$  for a trade-off.

### 6.4 Ablation Study

TABLE 4  
Ablation study of GFM on ORI-Track and COMP-Track.

Track	ORI				
Method	SAD	MSE	MAD	Grad	Conn
GFM-TT(d)	10.27	<b>0.0027</b>	<b>0.0060</b>	8.80	9.37
GFM-TT(r)	10.89	0.0029	0.0064	10.00	9.99
GFM-TT(r2b)	<b>10.24</b>	0.0028	<b>0.0060</b>	<b>8.65</b>	<b>9.33</b>
GFM-TT-SINGLE(d)	13.79	0.0040	0.0081	13.45	13.04
GFM-TT-SINGLE(r)	15.50	0.0040	0.0091	14.21	13.15
GFM-TT(d) excl. PPM	10.86	0.0030	0.0064	9.91	9.92
GFM-TT(d) excl. BB	11.27	0.0035	0.0067	9.33	10.40
GFM-TT(r) excl. PPM	11.90	0.0035	0.0070	10.50	11.07
GFM-TT(r) excl. BB	11.29	0.0032	0.0066	9.59	10.43
Track	COMP-RSSN				
GFM-TT(d)	25.19	0.0104	0.0146	15.04	24.31
GFM-TT(d) w/ blur	21.37	0.0081	0.0124	14.31	20.50
GFM-TT(d) w/ denoise	22.95	0.0090	0.0134	14.37	22.10
GFM-TT(d) w/ noise	19.87	0.0075	0.0116	<b>13.22</b>	18.97
GFM-TT(d) w/ RSSN	<b>19.19</b>	<b>0.0069</b>	<b>0.0112</b>	13.37	<b>18.31</b>

**Results on the ORI-Track.** To further verify the benefit of designed structure in GFM, we conducted ablation studies on several variants of GFM on AM-2k's ORI-Track including 1) motivated by Qin et.al [39], in GFM encoder when using ResNet-34 [35] as the backbone, we modified the convolution kernel of  $E_0$  from  $7 \times 7$  with stride 2 to  $3 \times 3$  with stride 1, removed the first max pooling layer in  $E_0$ , and added two more encoder layers  $E_5$  and  $E_6$  after  $E_4$ , each of which had a max pooling layer with stride 2 and three basic res-blocks with 512 filters, denoting "r2b"; 2) using a single decoder to replace both FD and GD in GFM, denoting "SINGLE"; 3) excluding the pyramid pooling module (PPM) in GD, and 4) excluding the bridge block(BB) in FD. The results are summarized in the top of Table 4. **First**, when using *r2b* structure, all the metrics have been improved compared with GFM-TT(r), which is attributed to the larger feature maps at the early stage of the encoder part. However, it has more parameters and computations than GFM-TT(r), which will be discussed later. **Second**, using only single decoder results in worse performance, *i.e.*, SAD increases from 10.27

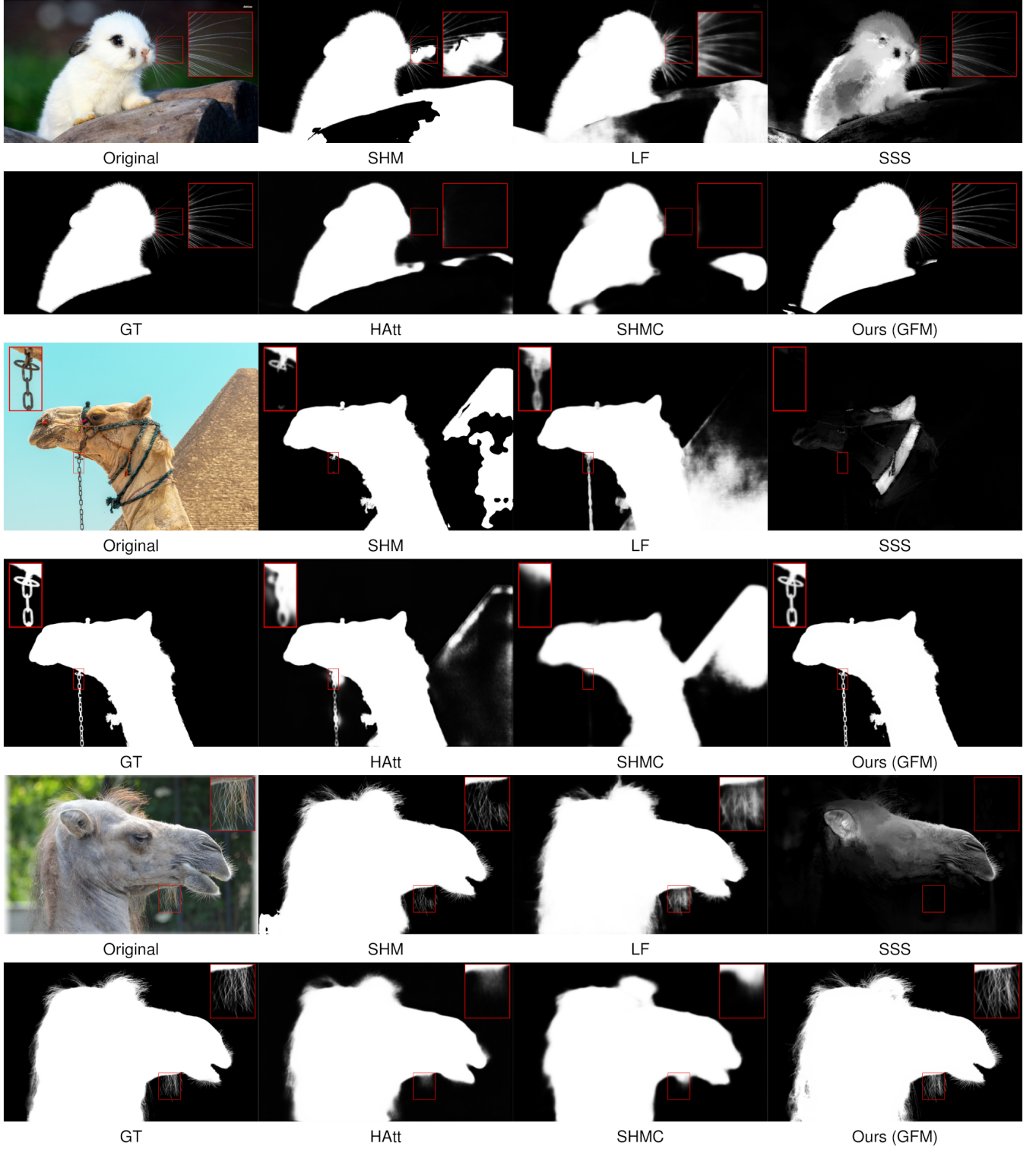


Fig. 6. Qualitative comparison of different methods on the AM-2k ORI-Track, including SHM [7], LF [8], SSS [12], HAtt [9], SHMC [10], and GFM.

to 13.79 for GFM-TT(d) and 10.89 to 15.50 for GFM-TT(r), which confirms the value of decomposing the end-to-end image matting task into two collaborative sub-tasks. **Third**, without PPM, SAD increases from 10.86 to 10.27 for GFM-TT(d) and 11.90 to 10.89 for GFM-TT(r), demonstrating that the global context features by PPM due to its larger receptive field are beneficial for semantic segmentation in GD. **Fourth**,

without BB, SAD increases from 10.27 to 11.27 for GFM-TT(d) and 10.89 to 11.29 for GFM-TT(r), demonstrating that the learned local structural features by BB due to its dilated convolutional layers are beneficial for matting in FD.

**Results on the COMP-Track.** In order to verify the different techniques in the proposed composition route RSSN, we conducted ablation studies on several variants of RSSN: 1) only using the simulation of large-aperture effect,

denoting “w/ blur”; 2) only removing foreground and background noise, denoting “w/ denoise”; 3) only adding noise on the composite images, denoting “w/ noise”; and 4) using all the techniques in RSSN, denoting “w/ RSSN”. We used the BG-20k for sampling background images in these experiments. The results are summarized at the bottom of Table 4. **First**, compared with the baseline model listed in the first row, which was trained using the composite images by alpha-blending, each technique in the proposed composition route is helpful to improve the matting performance in terms of all the metrics. **Second**, simulation of large-aperture effect and adding noise on the composite images are more effective than denoising. **Third**, different techniques are complementary to each other that they contribute to the best performance achieved by RSSN collaboratively.

## 6.5 Model Complexity Analysis

TABLE 5

Comparison of model parameters, computing complexity, and running time. (*d*) and (*r*) stand for DenseNet-121 [36] and ResNet-34 [35].

Method	Parameters (M)	Complexity (GMac)	Running time (s)
SHM [7]	79.27	870.16	0.3346
LF [8]	37.91	2821.14	0.3623
HAtt [9]	106.96	1502.46	0.5176
SHMC [10]	78.23	139.55	0.4863
GFM-TT(d)	46.96	244.0	0.2085
GFM-TT(r)	55.29	132.28	0.1734
GFM-TT(r2b)	126.85	1526.79	0.2268

We compared the number of model parameters (million, denoting “M”), computing complexity (denoting “GMac”), and inference time (seconds, denoting “s”) of each method on an image resized to  $800 \times 800$ . All methods are performed on a server with an Intel Xeon CPU (2.30GHz) and an NVIDIA Tesla V100 GPU (16GB memory). As shown in Table 5, GFM using either DenseNet-121 [36] or ResNet-34 [35] as the backbone surpasses SHM [7], LF [8], Hatt [9] and SHMC [10] in running speed, i.e., taking about 0.2085s and 0.1734s to process an image. In terms of parameters, GFM has fewer parameters than all the SOTA methods except for LF [8]. For computing complexity, GFM has fewer computations than all the SOTA methods when adopting ResNet-34 [35] as the backbone, i.e., 132.28 GMacs. When adopting DenseNet-121 [36], it only has more computations than SHMC [10] while being smaller. As for GFM(r2b), it has more parameters and computations. Although it can achieve better results, a trade-off between performance and complexity should be made for practical applications. Generally, GFM is light-weight and computationally efficient.

## 7 CONCLUSION AND FUTURE WORKS

In this paper, we propose a novel image matting model for natural animal image matting. It addresses two challenges in this matting problem: 1) recognizing various foreground animals with diverse shapes, sizes, and textures from different categories; and 2) extracting fur details from ambiguous context background. Specifically, a Glance Decoder is devised for the first task and a Focus Decoder is devised for

the latter one, while they share an encoder and are trained jointly. Therefore, they collaboratively accomplish the end-to-end animal matting task and achieve superior performance than state-of-the-art matting methods. Besides, we also point out the domain discrepancy between composite images and natural ones which suggests that the common practice for data augmentation may not be suitable for training end-to-end matting models. To remedy this issue, we establish the first large-scale natural animal image matting dataset, which contains 2,000 high-resolution animal images from 20 categories and manually labeled alpha mattes. We also construct a background dataset containing 20,000 high-resolution images without salient objects. Furthermore, we systematically analyze the factors affecting composition quality and propose a novel composition route, which can effectively address the domain discrepancy issue. Extensive experiments validate the superiority of the proposed methods over state-of-the-art methods. We believe the proposed matting method and composition route will benefit the research for both trimap-based and end-to-end image matting. Moreover, the proposed dataset can provide a testbed to study the matting problem including the domain discrepancy issue.

Although GFM outperforms state-of-the-art methods in terms of both objective metrics and subjective evaluation, there are some limitations to be addressed in future work. First, after taking a detailed analysis of the error source as evidenced by SAD-TRAN, SAD-FG, and SAD-BG, the error in the transition areas is larger than in that in the foreground and background areas, i.e., 8.45 v.s. 1.83, even if the size of transition areas is usually much smaller than that of foreground and background areas. It tells that the performance could be further enhanced by devising a more effective Focus Decoder as well as leveraging some structure-aware and perceptual losses. Second, there is still room to improve for the composite-based model since the cost required to generate a composite-based training set is much easier than constructing a natural images-based one. Given that alpha matting and alpha blending are inverse problems, it is interesting to see whether or not these two tasks benefit each other if we model them in a single framework. Third, it is interesting to investigate the impact of synthesizing appearance-like composite images as natural ones to reduce the domain gap and augmentation techniques to avoid overfitting as well as their differences in improving the generalization ability of matting models.

## REFERENCES

- [1] Ning Xu, Brian Price, Scott Cohen, and Thomas Huang. Deep image matting. In *Proceedings of the IEEE Conference on Computer Vision and Pattern Recognition*, pages 2970–2979, 2017.
- [2] Anat Levin, Dani Lischinski, and Yair Weiss. A closed-form solution to natural image matting. *IEEE Transactions on Pattern Analysis and Machine Intelligence*, 30(2):228–242, 2007.
- [3] Jue Wang and Michael F Cohen. Optimized color sampling for robust matting. In *Proceedings of the IEEE Conference on Computer Vision and Pattern Recognition*, pages 1–8, 2007.
- [4] Mark A Ruzon and Carlo Tomasi. Alpha estimation in natural images. In *Proceedings IEEE Conference on Computer Vision and Pattern Recognition*, pages 18–25, 2000.
- [5] Jue Wang and Michael F Cohen. An iterative optimization approach for unified image segmentation and matting. In *Proceedings of the IEEE International Conference on Computer Vision*, pages 936–943, 2005.



- [6] Yuanjie Zheng, Chandra Kambhampati, Jingyi Yu, Thomas Bauer, and Karl Steiner. Fuzzymatte: A computationally efficient scheme for interactive matting. In *Proceedings IEEE Conference on Computer Vision and Pattern Recognition*, pages 1–8, 2008.
- [7] Quan Chen, Tiezheng Ge, Yanyu Xu, Zhiqiang Zhang, Xinxin Yang, and Kun Gai. Semantic human matting. In *Proceedings of the ACM International Conference on Multimedia*, pages 618–626, 2018.
- [8] Yunke Zhang, Lixue Gong, Lubin Fan, Peiran Ren, Qixing Huang, Hujun Bao, and Weiwei Xu. A late fusion cnn for digital matting. In *Proceedings of the IEEE Conference on Computer Vision and Pattern Recognition*, pages 7469–7478, 2019.
- [9] Yu Qiao, Yuhao Liu, Xin Yang, Dongsheng Zhou, Mingliang Xu, Qiang Zhang, and Xiaopeng Wei. Attention-guided hierarchical structure aggregation for image matting. In *Proceedings of the IEEE Conference on Computer Vision and Pattern Recognition*, 2020.
- [10] Jinlin Liu, Yuan Yao, Wendi Hou, Miaomiao Cui, Xuansong Xie, Changshui Zhang, and Xian-sheng Hua. Boosting semantic human matting with coarse annotations. In *Proceedings of the IEEE Conference on Computer Vision and Pattern Recognition*, pages 8563–8572, 2020.
- [11] Xiaoyong Shen, Xin Tao, Hongyun Gao, Chao Zhou, and Jiaya Jia. Deep automatic portrait matting. In *Proceedings of the European Conference on Computer Vision*, pages 92–107, 2016.
- [12] Yağiz Aksoy, Tae-Hyun Oh, Sylvain Paris, Marc Pollefeys, and Wojciech Matusik. Semantic soft segmentation. *ACM Transactions on Graphics*, 37(4):1–13, 2018.
- [13] Christoph Rhemann, Carsten Rother, Jue Wang, Margrit Gelautz, Pushmeet Kohli, and Pamela Rott. A perceptually motivated online benchmark for image matting. In *Proceedings of the IEEE Conference on Computer Vision and Pattern Recognition*, pages 1826–1833, 2009.
- [14] Tsung-Yi Lin, Michael Maire, Serge Belongie, James Hays, Pietro Perona, Deva Ramanan, Piotr Dollár, and C Lawrence Zitnick. Microsoft coco: Common objects in context. In *Proceedings of the European Conference on Computer Vision*, pages 740–755, 2014.
- [15] Mark Everingham, Luc Van Gool, Christopher KI Williams, John Winn, and Andrew Zisserman. The pascal visual object classes (voc) challenge. *International Journal of Computer Vision*, 88(2):303–338, 2010.
- [16] Yung-Yu Chuang, Brian Curless, David H Salesin, and Richard Szeliski. A bayesian approach to digital matting. In *Proceedings of the IEEE Conference on Computer Vision and Pattern Recognition*, 2001.
- [17] Jian Sun, Jiaya Jia, Chi-Keung Tang, and Heung-Yeung Shum. Poisson matting. *ACM Transactions on Graphics*, 23(3):315–321, 2004.
- [18] Anat Levin, Alex Rav-Acha, and Dani Lischinski. Spectral matting. *IEEE Transactions on Pattern Analysis and Machine Intelligence*, 30(10):1699–1712, 2008.
- [19] Qifeng Chen, Dingzeyu Li, and Chi-Keung Tang. Knn matting. *IEEE Transactions on Pattern Analysis and Machine Intelligence*, 35(9):2175–2188, 2013.
- [20] Hao Lu, Yutong Dai, Chunhua Shen, and Songcen Xu. Indices matter: Learning to index for deep image matting. In *Proceedings of the IEEE International Conference on Computer Vision*, pages 3266–3275, 2019.
- [21] Qiqi Hou and Feng Liu. Context-aware image matting for simultaneous foreground and alpha estimation. In *Proceedings of the IEEE International Conference on Computer Vision*, pages 4130–4139, 2019.
- [22] Shaofan Cai, Xiaoshuai Zhang, Haoqiang Fan, Haibin Huang, Jiangyu Liu, Jiaming Liu, Jiaying Liu, Jue Wang, and Jian Sun. Disentangled image matting. In *Proceedings of the IEEE International Conference on Computer Vision*, pages 8819–8828, 2019.
- [23] Jingwei Tang, Yağiz Aksoy, Cengiz Oztireli, Markus Gross, and Tunc Ozan Aydin. Learning-based sampling for natural image matting. In *Proceedings of the IEEE Conference on Computer Vision and Pattern Recognition*, pages 3055–3063, 2019.
- [24] Su Xue, Aseem Agarwala, Julie Dorsey, and Holly Rushmeier. Understanding and improving the realism of image composites. *ACM Transactions on Graphics*, 31(4):1–10, 2012.
- [25] Yi-Hsuan Tsai, Xiaohui Shen, Zhe Lin, Kalyan Sunkavalli, Xin Lu, and Ming-Hsuan Yang. Deep image harmonization. In *Proceedings of the IEEE Conference on Computer Vision and Pattern Recognition*, pages 3789–3797, 2017.
- [26] Bor-Chun Chen and Andrew Kae. Toward realistic image compositing with adversarial learning. In *Proceedings of the IEEE Conference on Computer Vision and Pattern Recognition*, pages 8415–8424, 2019.
- [27] Wenyang Cong, Jianfu Zhang, Li Niu, Liu Liu, Zhixin Ling, Weiyan Li, and Liqing Zhang. Dovenet: Deep image harmonization via domain verification. In *Proceedings of the IEEE Conference on Computer Vision and Pattern Recognition*, pages 8394–8403, 2020.
- [28] Soumyadip Sengupta, Vivek Jayaram, Brian Curless, Steven M Seitz, and Ira Kemelmacher-Shlizerman. Background matting: The world is your green screen. In *Proceedings of the IEEE Conference on Computer Vision and Pattern Recognition*, pages 2291–2300, 2020.
- [29] Qi Wang, Junyu Gao, Wei Lin, and Yuan Yuan. Learning from synthetic data for crowd counting in the wild. In *Proceedings of the IEEE Conference on Computer Vision and Pattern Recognition*, pages 8198–8207, 2019.
- [30] Debidatta Dwibedi, Ishan Misra, and Martial Hebert. Cut, paste and learn: Surprisingly easy synthesis for instance detection. In *Proceedings of the IEEE International Conference on Computer Vision*, pages 1301–1310, 2017.
- [31] Yuhua Chen, Wen Li, Xiaoran Chen, and Luc Van Gool. Learning semantic segmentation from synthetic data: A geometrically guided input-output adaptation approach. In *Proceedings of the IEEE Conference on Computer Vision and Pattern Recognition*, pages 1841–1850, 2019.
- [32] Swami Sankaranarayanan, Yogesh Balaji, Arpit Jain, Ser Nam Lim, and Rama Chellappa. Learning from synthetic data: Addressing domain shift for semantic segmentation. In *Proceedings of the IEEE Conference on Computer Vision and Pattern Recognition*, pages 3752–3761, 2018.
- [33] Patrick Pérez, Michel Gangnet, and Andrew Blake. Poisson image editing. In *ACM SIGGRAPH*, pages 313–318, 2003.
- [34] Nikolaus Mayer, Eddy Ilg, Philipp Fischer, Caner Hazirbas, Daniel Cremers, Alexey Dosovitskiy, and Thomas Brox. What makes good synthetic training data for learning disparity and optical flow estimation? *International Journal of Computer Vision*, 126(9):942–960, 2018.
- [35] Kaiming He, Xiangyu Zhang, Shaoqing Ren, and Jian Sun. Deep residual learning for image recognition. In *Proceedings of the IEEE Conference on Computer Vision and Pattern Recognition*, pages 770–778, 2016.
- [36] Gao Huang, Zhuang Liu, Laurens Van Der Maaten, and Kilian Q Weinberger. Densely connected convolutional networks. In *Proceedings of the IEEE Conference on Computer Vision and Pattern Recognition*, pages 4700–4708, 2017.
- [37] Hengshuang Zhao, Jianping Shi, Xiaojuan Qi, Xiaogang Wang, and Jiaya Jia. Pyramid scene parsing network. In *Proceedings of the IEEE Conference on Computer Vision and Pattern Recognition*, pages 2881–2890, 2017.
- [38] Jiang-Jiang Liu, Qibin Hou, Ming-Ming Cheng, Jiashi Feng, and Jianmin Jiang. A simple pooling-based design for real-time salient object detection. In *Proceedings of the IEEE Conference on Computer Vision and Pattern Recognition*, 2019.
- [39] Xuebin Qin, Zichen Zhang, Chenyang Huang, Chao Gao, Masood Dehghan, and Martin Jagersand. Basnet: Boundary-aware salient object detection. In *Proceedings of the IEEE Conference on Computer Vision and Pattern Recognition*, 2019.
- [40] Olaf Ronneberger, Philipp Fischer, and Thomas Brox. U-net: Convolutional networks for biomedical image segmentation. In *International Conference on MICCAI*, pages 234–241, 2015.
- [41] Alex Krizhevsky, Ilya Sutskever, and Geoffrey E Hinton. Imagenet classification with deep convolutional neural networks. In *Advances in Neural Information Processing Systems*, pages 1097–1105, 2012.
- [42] Joseph Redmon and Ali Farhadi. Yolov3: An incremental improvement. *arXiv preprint arXiv:1804.02767*, 2018.
- [43] Kostadin Dabov, Alessandro Foi, Vladimir Katkovnik, and Karen Egiazarian. Bm3d image denoising with shape-adaptive principal component analysis. In *SPARS’09-Signal Processing with Adaptive Sparse Structured Representations*, 2009.
- [44] Liang-Chieh Chen, George Papandreou, Iasonas Kokkinos, Kevin Murphy, and Alan L Yuille. Deeplab: Semantic image segmentation with deep convolutional nets, atrous convolution, and fully connected crfs. *IEEE Transactions on Pattern Analysis and Machine Intelligence*, 40(4):834–848, 2017.